# Design of Photonic Crystal Nanocavity With $Q$-Factor of $\sim 10^9$

Yoshinori Tanaka, Takashi Asano, and Susumu Noda, *Fellow, IEEE*

*Invited Paper*

***Abstract*—Photonic crystal nanocavities are expected to make great contributions in areas of physics and engineering such as the slowing and stopping of light and optical quantum information processing. We first review approaches to the goal of increasing the quality factor of two-dimensional photonic crystal nanocavities. Losses from a cavity can be suppressed, with a consequent increase of the quality factor, by containing the electromagnetic field in the form of a Gaussian envelope function. We then propose a new method of analytical cavity design, based on the detailed investigation of waveguide modes, in order to realize Gaussian cavity mode fields. This has enabled us to achieve a quality factor of $\sim 10^9$ while maintaining a cavity volume of one cubic wavelength.**

***Index Terms*—Analytic continuation, design, Gaussian, modal volume, nanocavity, photonic crystal, Q factor, resonator.**

## I. Introduction

TWO-DIMENSIONAL (2D) photonic crystal (PC) nanocavities [1]–[9] are currently the focus of much interest because they are able to strongly confine photons within a tiny space. Even though these cavities have modal volumes of as small as a cubic wavelength, theoretical quality $(Q)$ factors more than 10 000 000 have been designed [3]–[5]. Correspondingly, the experimental $Q$-factor more than 2 000 000, the highest recorded value for any photonic crystal thus far, has been achieved [6], [7]. Moreover, dynamic control of such high $Q$-factor of a nanocavity has recently been both proposed and demonstrated [10]. It is expected that nanocavities will be applied to various areas of physics and engineering such as the slowing and/or stopping of light [10], [11], ultimate nanolasers [9], [12], [13], ultra-compact filters [14]–[16], and quantum information processing [6], [17], [18].

Manuscript received December 11, 2007; revised April 2, 2008. This work was supported in part by the Research Programs (Grant-in-Aid, COE, and Special Coordination Fund) for Scientific Research from the Ministry of Education, Culture, Sports, Science and Technology of Japan and in part by the Core Research for Evolutional Science and Technology of the Japan Science and Technology Agency.

Y. Tanaka and T. Asano are with the Department of Electronic Science and Engineering, Kyoto University, Kyoto 615-8510, Japan (e-mail: ytanaka@qoe.kuee.kyoto-u.ac.jp).

S. Noda is with the Department of Electronic Science and Engineering and the Center of Excellence for Education and Research on Photonics and Electronics Science and Engineering, Kyoto University, Kyoto 615-8510, Japan (e-mail: snoda@kuee.kyoto-u.ac.jp).

Color versions of one or more of the figures in this paper are available online at http://ieeexplore.ieee.org.

Digital Object Identifier 10.1109/JLT.2008.923648

In order to realize high-$Q$ cavities in a 2D PC, the main issue to consider is how strongly the photons can be confined in the out-of-plane direction by total internal reflection (TIR). We have previously reported an important design concept for the realization of high-$Q$ nanocavities: to suppress radiation loss, the envelope of the cavity mode field should be a Gaussian function [1], [2], [3], [6]. In this paper, we first explain the relationship between the Gaussian mode field and the-$Q$ factor, and review the design and characteristics of the cavities that we have developed. We then discuss a new analytical design for the realization of a Gaussian mode field by investigating the dispersion curve of the PC waveguide. Finally, we show the results of simulations for a cavity with a theoretical $Q$-factor of almost $10^9$ developed using this design concept.

## II. Review of Importance of Gaussian Confinement to Achieve High$Q$-Factor

In a 2D PC nanocavity, three-dimensional (3D) photon confinement is achieved using the photonic band gap (PBG) effect for the in-plane direction and by TIR for the vertical direction. Although perfect confinement within the in-plane direction can easily be achieved by using a sufficient number of PC periods, confinement of the localized mode in the out-of-plane direction is generally incomplete. Therefore, the most important issue to be addressed is how strongly the photons can be confined by TIR.

Initial designs used the combination of a donor-type defect, which consists of buried lattice points for the purpose of increasing the degree of TIR [19], [20], and a cavity with a gradual change of lattice point radius [21]. However, no clear direct design rules for improving the $Q$-factor were laid down until 2003, when we proposed the concept of Gaussian confinement [1]. In order to explain the way in which this mechanism is able to suppress losses, we consider the one-dimensional cavity shown in Fig. 1(a), whose structure is assumed to be uniform in the $y$ direction, normal to the paper. The model cavity consists of a dielectric material with finite length ($x$ direction) and thickness ($z$ direction); perfect mirrors enclose the cavity on both sides. We consider two extreme cavities with the same size and resonant wavelength, but different in-plane confinement characteristics. Photons in the first cavity are confined by sharp reflection at the cavity edges, giving a cavity mode electric field profile with a rectangular envelope function [Fig. 1(b)]. In the second cavity, photons are confined by spatially distributed reflection, such that the electric field profile of the cavity mode has a Gaussian envelope function [Fig. 1(c)]. These electric field

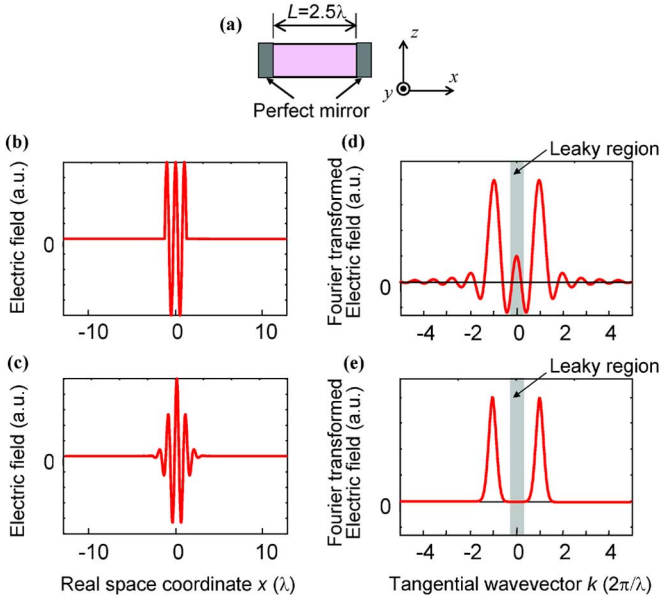


Fig. 1. Analysis of cavities with different in-plane confinement characteristics. (a) Simplified model of a cavity. Electric field profiles of cavities with (b) a rectangular envelope function, and (c) a Gaussian envelope function. (d) and (e) Respective Fourier transform spectra of (b) and (c).

profiles are taken along the interfaces between the slabs and cladding (air) of the cavities, but each profile is valid for all $z$-positions inside its respective cavity. The real space coordinate is given in units of the wavelength of the resonant mode inside the cavity $(\lambda)$. Fig. 1(d) and (e) show the spatial Fourier transform (FT) spectra of each electric field profile, which represent the plane wave components of the cavity mode. The horizontal axis represents the wavevector tangential to the interface $(k_{//})$. The wavevector of light propagating through the cladding is $k_0$; only plane wave components with $|k_{//}| > k_0$ can be confined by TIR. The gray regions in Fig. 1(d) and (e) represent the region where $|k_{//}| < k_0$, that is, the "leaky region," where the plane wave components of a cavity mode are radiated into the cladding. It is apparent that the cavity with the rectangular envelope function [Fig. 1(b) and (d)] has a greater plane wave component inside the leaky region than the cavity with the Gaussian envelope function [Fig. 1(c) and (e)].

Understanding the difference between the two types of cavity modes is considered to be vital for the realization of high-$Q$ photonic nanocavities. We analyzed the cavity mode electric field profiles by separating them into a fundamental sinusoidal wave with a wavelength of $\lambda$ and an envelope function. The mode field profile is then expressed as the product of the fundamental wave and the envelope function in real space, while the FT spectrum of the mode field profile is described by a convolution of the FT spectra of the fundamental wave and the envelope function. The FT of the fundamental wave gives two delta functions at $k_{//} = \pm 2\pi/\lambda$, and the FT of the envelope gives a function of finite width that depends on its shape in real space. Since the FT of the fundamental wave is outside the leaky region, the component within the leaky region is generated by the convolution with the envelope spectrum. The convolution of the two delta functions and the envelope spectrum is the sum of two envelope spectra, shifted by $+2\pi/\lambda$ and $-2\pi/\lambda$. Therefore, the higher spatial frequency components of the envelope spectrum, with $(2\pi/\lambda - k_0) < |k_{//}| < (2\pi/\lambda + k_0)$, are transferred to the leaky region. The FT mode electric field profile associated with the rectangular envelope function [Fig. 1(b) and (d)] has a large component in the higher spatial frequency region, due to the abrupt changes in the envelope function at both edges. This results in large radiation losses. In contrast, the mode electric field profile associated with the Gaussian envelope function [Fig. 1(c) and (e)] has only a small component in the higher spatial frequency region, due to the smooth variation of the envelope function in real space. Therefore, only small radiation losses are suffered. It is clear that the shape of the envelope function has a critical effect on the radiation loss of the model cavity and that abrupt changes in the envelope function should be avoided in order to obtain high $Q$-factors. The confinement of light within regions with dimensions of the order of optical wavelengths requires a spatially localized envelope function of the same dimensions. In order to realize a high-$Q$ photonic nanocavity, the envelope function should be spatially localized but have no high-frequency components. As shown here, a Gaussian function can fulfill both these requirements and thus a Gaussian function is practically ideal function for designing a high-$Q$ photonic nanocavity.

On the basis of the above considerations, we designed a high-$Q$ photonic nanocavity in a 2D PC based on the L3 cavity shown in Fig. 2(a), which was created by burying three air rods in a line along the $\Gamma - \mathrm{J}$ direction (parallel to the $x$-direction in this structure). The thickness of the slab, the radius of the air rods and the refractive index of the slab were $0.6a, 0.29a$ and 3.4, respectively. The electric field profile, $E_y$, of the fundamental mode of the cavity was calculated using the 3D finite-difference time-domain (FDTD) method, and is shown in Fig. 2(b). To simplify the analysis of the calculated profile, we focused on $E_y$ for the centerline of the cavity along the $x$-direction in real space [solid line in Fig. 2(a)]. We fitted the mode field profile using a curve corresponding to the product of a sinusoidal wave, with a wavelength the same as that of the fundamental wave of the $E_y$ profile, and a Gaussian function [dashed line in Fig. 2(b)]. The fitted curve closely matches $E_y$ near the center of the cavity, but at the edges of the cavity [indicated by dashed circles in Fig. 2(b)], the envelope of $E_y$ decreases more rapidly than the Gaussian function.

In order to bring the cavity mode profile closer to the ideal Gaussian function, the air-holes at the cavity edges were shifted to lay $0.2a$ outside the cavity [1]. The resulting cavity structure and calculated electric field distribution are shown in Fig. 2(c). The $E_y$ profile along the centerline [solid line in Fig. 2(c)] is shown in Fig. 2(d) together with the fitted curve, generated in the same manner as described above. This structural adjustment resulted in weaker reflection at the cavity edges, as the periodicity of the air holes is disturbed. Therefore, the PBG effect is also expected to be weakened. As shown in Fig. 2(d), the electric field profile of the modified cavity is closer to the Gaussian curve than that of the original cavity without displacement of air-holes. The calculated $Q$-factor of the cavity shown in Fig. 2(c) is 100 000, which is 20 times larger than that of the cavity with no air hole shifts. We fabricated this cavity and obtained an experimental $Q$-factor of 45000.

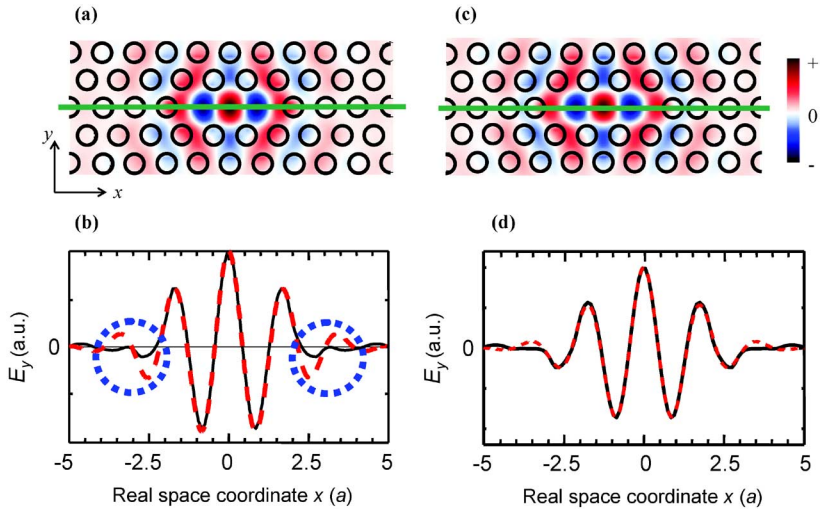


Fig. 2. (a) Calculated $E_y$ electric field distribution of the fundamental resonant mode of the L3 cavity with no air-hole shift. (b) $E_y$ profile along the centerline of the cavity in the $x$ direction (solid line) and a fitted curve calculated using the same fundamental wave and a Gaussian envelope function (dashed line). (c) $E_y$ for the cavity with an air-hole shift of $0.2a$. (d) $E_y$ profile along the centerline of the cavity with an air-hole shift (solid line) and a fitted curve obtained in the same fashion as (b) (dashed line).

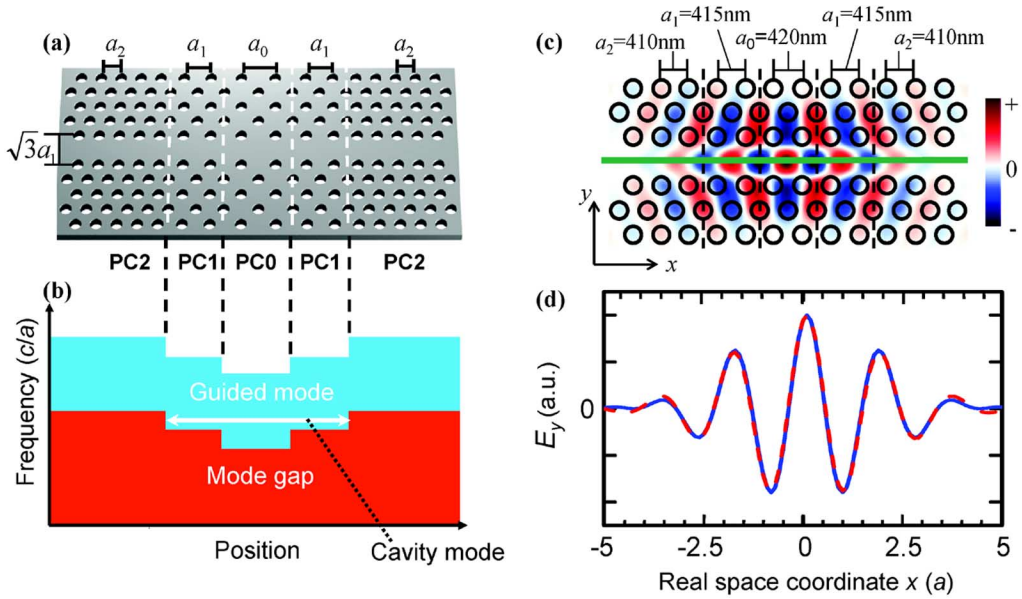


Fig. 3. (a) Schematic image of a multiheterostructure nanocavity. (b) Schematic picture of the band diagram along the waveguide direction. Photons of a specific energy (white arrow) can exist only in the waveguide of PC0 and PC1. (c) Calculated $E_y$ distribution in the photonic multiheterostructure nanocavity, and (d) $E_y$ profile along the waveguide direction. Solid and dashed lines indicate calculated results and the ideal Gaussian profile, respectively.

In 2005, we proposed the concept of "photonic multiheterostructures" as a more comprehensive method to tune the envelope function of a cavity [3]. In Fig. 3(a), three PCs (0, 1 and 2) with a common line defect are joined to form a double heterostructure. The lattice constants of PC0 $(a_0)$, PC1 $(a_1)$ and PC2 $(a_2)$ are in the order $a_0 > a_1 > a_2$. The transmission frequency range of the line defect varies with the lattice constant [Fig. 3(b)], ensuring that light with a frequency slightly above the mode edge of PC1 becomes a propagation mode in the line defect in both PC0 and PC1 and is in the mode-gap region of the waveguide, where the propagation mode does not exist but evanescent modes can be excited. The calculated electric-field distribution of the photonic double-heterostructure cavity and its profile along the waveguide direction are shown in Fig. 3(c) and (d), respectively. The calculation was performed using the 3-D FDTD method, where the lattice constants of PCs 0, 1 and 2 were $a_0 = 420$ nm, $a_1 = 415$ nm, and $a_2 = 410$ nm, respectively, and the slab thickness was $0.6a_0$. In Fig. 3(d), the solid and dashed lines indicate the calculated electric field distribution and the fitted curve, generated as described above, respectively. The electric field profile of the photonic multiheterostructure cavity lay very close to the ideal Gaussian curve. For an air hole radius of 0.26 $a_0$, the maximum theoretical $Q$-factor exceeded 24 000 000 and the modal volume of the cavity was $\sim 1.2(\lambda_0/n)^3$. We have recently succeeded in fabricating this type of photonic multiheterostructure nanocavity, achieving a $Q$-factor of more than $2 \times 10^6$ by careful optimization of the fabrication process [6], [7]. This represents the

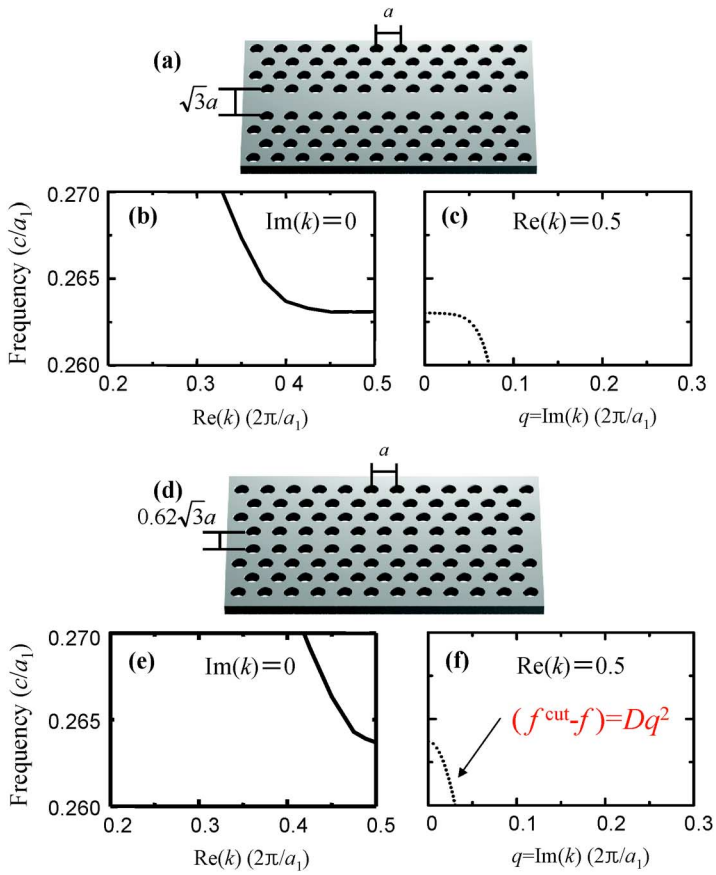


Fig. 4. (a) Schematic picture of a waveguide with width $W = \sqrt{3}a$. (b) Calculated dispersion relation of a propagation mode for waveguide in (a). (c) Dispersion relation of the mode-gap, calculated from (b). (d) Schematic picture of a PC1 waveguide with width $W = 0.62 \times \sqrt{3}a$. (e) Calculated dispersion relation of a propagation mode for waveguide in (d). (f) Dispersion relation of the mode-gap, calculated from (e).

highest recorded experimental $Q$-factor for any PC nanocavity to date. Note that this concept of multiheterostructure cavity has various variations. For example, waveguide widths' modulation [5] instead of lattice-constant modulation can be utilized to achieve the band structure as shown in Fig. 3(b).

## III. New Design for Realization of Gaussian Mode Field With $Q$-Factor of $10^9$

In Section II, we demonstrate that a cavity mode field with a Gaussian envelope is the key requirement for realizing a high-$Q$ photonic nanocavity, and we describe a multiheterostructure nanocavity that fulfills the necessary conditions. However, the analytical design rule for obtaining a Gaussian mode field has not been discussed. In this section, we develop a straightforward, analytical cavity design that produces Gaussian mode fields by studying the dispersion curve of a PC waveguide. The Gaussian mode field is of the form $\exp(-Bx^2)$, where $x$ represents the distance from the center of the cavity, and $B$ is a constant. To realize this mode shape, we consider building a cavity that uses the mode-gap region of PC waveguides. The evanescent mode field in the mode-gap region diminishes exponentially and can be expressed as $\exp(-qx)$, where $q$ is the imaginary part of wavevector $k(q = \mathrm{Im}(k))$, which gives the decay of the mode field. Therefore, the condition

$$q = Bx \tag{1}$$

should be satisfied for a Gaussian mode field. That is, $q$ should be proportional to $x$.

For the design of this cavity, the dispersion diagram of the mode-gap region of the waveguide is required, and is calculated in Section III-A. In Section III-B, a cavity with a Gaussian mode field is designed according to the calculated dispersion diagram. In Section III-C, the properties of the cavity are investigated using FDTD calculations.

### *A. Dispersion of Evanescent Wave in Photonic Crystal Waveguide*

The dispersion diagram of the evanescent wave near the band edge can be derived from the extension of the dispersion curve of the allowed band (waveguide mode) using the analytic continuation method [22], [23]. Fig. 4(a) shows a schematic picture of a waveguide of width $W = \sqrt{3}a$, which corresponds to one buried row of air holes in the $\Gamma - J$ direction. The waveguide width $W$ is defined as the distance between the centers of the air holes in the rows on each side of the waveguide. The radius of the air holes is $0.29a$ and the slab thickness is $0.6a$. The dielectric slab is assumed to be composed of silicon $(n = 3.4)$. The dispersion relation of a propagation mode of this waveguide, calculated using the 3D FDTD method, is shown in Fig. 4(b). This dispersion function can be fitted using a Taylor series expansion of the term $(k - 0.5)$. We consider only the even-order

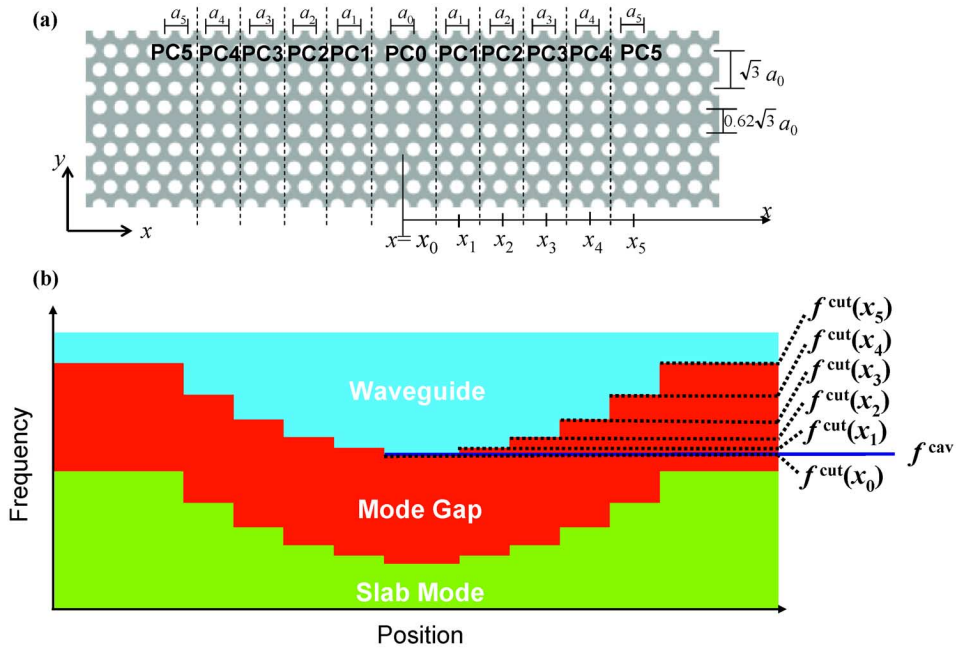


Fig. 5. (a) Schematic picture of multiheterostructure nanocavity based on refractive index guiding waveguide. (b) Schematic picture of the band diagram along the waveguide direction.

terms because the dispersion relation is even at the Brillouin zone boundary ($k = 0.5$). The fitted function is expressed as

$$f = 0.263 + 0.01(k-0.5)^2 + 2.5(k-0.5)^4 + 200(k-0.5)^6. \quad (2)$$

It is apparent that not only the second-order term $(k-0.5)^2$ but also fourth- and sixth-order terms are necessary to fit the dispersion curve near the mode-edge frequency. This is because the slope of the dispersion curve near the mode-edge is unusually small, due to the fact that the guiding mechanism of this waveguide is not refractive index guiding but rather PBG guiding. The imaginary dispersion relation for the mode-gap region can be derived using the analytic continuation method by substituting the complex wavevector $k = 0.5 + iq$ into (2). The resulting dispersion curve in the mode-gap region is shown in Fig. 4(c) and is expressed as

$$f = 0.263 - 0.01q^2 + 2.5q^4 - 200q^6. \quad (3)$$

This is not a parabolic function but is similar to a step function. Although such a step-like dispersion curve allows a double-heterostructure cavity with a small modal volume and a small variation in lattice constants, the function is too complex to enable straightforward analytic cavity design.

In order to obtain a simpler dispersion curve, we adopt a waveguide with refractive index guiding, as is present in conventional dielectric waveguides. We consider the waveguide shown in Fig. 4(d), which differs from that in Fig. 4(a) only in width $(W = 0.62 \times \sqrt{3}a)$ [23]. The dispersion relation of the propagation mode of this waveguide was calculated using a similar procedure to that described above, and is shown in Fig. 4(e). It can be fitted by the function

$$f = 0.263 + 0.94(k-0.5)^2. \quad (4)$$

Unlike (1), only the second-order term in $(k-0.5)^2$ is necessary to fit the dispersion relation of this propagation mode. This is because refractive index guiding is the relevant mechanism here, as found in conventional dielectric waveguides. Substituting $k = 0.5 + iq$ into (4), the complex dispersion relation of the waveguide in the mode-gap region is obtained and expressed as

$$f = 0.263 - 0.94q^2. \quad (5)$$

This parabolic function is shown in Fig. 4(f), and enables simpler analytic cavity design.

### *B. Multiheterostructure Cavity Design for Realization of Gaussian Mode Field Using Refractive Index Guiding Waveguide*

We will now discuss the analytic design of nanocavities possessing a Gaussian mode field by using the dispersion curve in the mode-gap region obtained in Section III-B. For the realization of a high-$Q$ nanocavity, $q$ should be

$$q = Bx \quad (6)$$

as shown in Section III-A. The damping factor of the waveguide in the mode-gap region can then be derived by substituting $f = f^{cav}$ in (5)

$$f^{cav} = f^{cut} - Aq^2. \quad (7)$$

Here, $f^{cut}$ is the cutoff frequency of the waveguide ($f^{cut} = 0.263\,c/a$) and $A$ is a constant ($A = 2.5$). Combining (6) and (7) gives

$$f^{cut}(x) - f^{cav} = AB^2x^2. \quad (8)$$

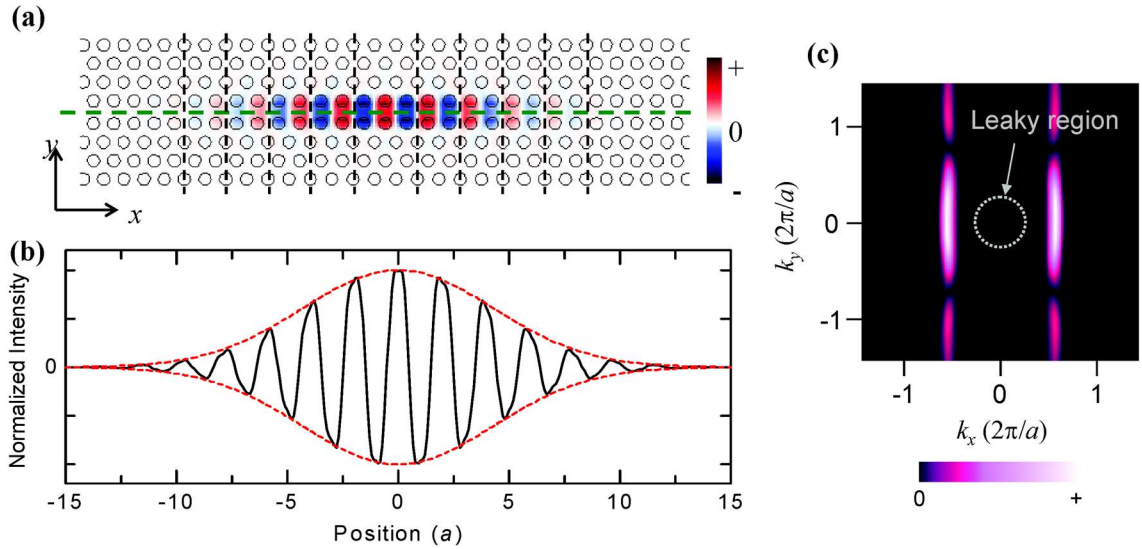


Fig. 6. (a) Calculated $E_y$ distribution of the fundamental resonant mode of the new multiheterostructure nanocavity based on a refractive index guiding waveguide. (b) $E_y$ profile along the centerline of the cavity in the $x$ direction (solid line) and fitted Gaussian envelope function (dashed line). (c) 2-D Fourier transform spectra of the $E_y$ electric field profile for this cavity mode.

Here, $f^{\rm cut}(x)$ is the cutoff frequency at position $x$. This implies that the cutoff frequency is variable, which can be achieved by use of the multiheterostructure shown in Fig. 5(a). Five different lattice constants are used in this structure: PC0 extends over 3 lattice constants, PC1 to PC4 each extend over 2 lattice constants, and PC5 is considered to be semi-infinite in length. The band structure of this defect should be Fig. 5(b), where $\{f^{\rm cut}(x) - f^{\rm cav}\}$ is proportional to the square of $x$.

The cutoff frequency $f^{\rm cut}$ is inversely proportional to the lattice constant because the operating wavelength of a PC, including the cutoff wavelength, is proportional to the lattice constant. Therefore, the cutoff frequency $f^{\rm cut}(x)$ and the lattice constant $a(x)$ at a position $x$ should satisfy

$$f(x)^{\rm cut} = \frac{a_0}{a(x)} f_0^{\rm cut} \tag{9}$$

where $f_0^{\rm cut}$ and $a_0$ represent the cutoff frequency and lattice constant of PC0, respectively. By assuming that the resonant frequency of the designed cavity $f^{\rm cav}$ is equal to $f_0^{\rm cut}$, $a(x)$ can be derived from (8) and (9) as

$$a(x) = \frac{a_0}{1 + AB^2x^2/f_0^{\rm cut}}. \tag{10}$$

When the condition $(AB^2x^2/f_0^{\rm cut}) << 1$ is satisfied

$$a(x) = a_0(1 - AB^2x^2/f_0^{\rm cut}). \tag{11}$$

As shown in Fig. 5(a), the distance $x_n$ between the center of the cavity and the center of $\rm PC_n$ for $n = 1$ to 4 can be approximated as

$$x_n = (2n + 1/2)a_0 \tag{12}$$

by assuming that the change in lattice constants is small. Substituting (12) into (11) gives

$$a_n = a_0\{1 - 4AB^2a_0^2(n + 1/4)^2/f_0^{\rm cut}\}. \tag{13}$$

Taking $C = 4AB^2a_0^2/f_0^{\rm cut}$, this expression can be simplified to

$$a_n = a_0\{1 - C(n + 1/4)^2\}. \tag{14}$$

Equation (14) gives us the required lattice constants for each $\rm PC_n (n = 1$ to $5)$ in order to realize a cavity with a Gaussian mode field.

### *C. FDTD Analysis of Newly Designed Multiheterostructure Nanocavity*

We carried out 3D FDTD calculations for a cavity with $C = 1.45 \times 10^{-3} (a_1 = 0.998a_0, a_2 = 0.993a_0, a_3 = 0.985a_0, a_4 = 0.974a_0$, and $a_5 = 0.960a_0)$. The cell size in the FDTD calculation is set to be $0.1a_0$. The $Q$ factor is calculated by the ratio of the electromagnetic energy in the cavity and flux of enegy exiting the cavity to free space. The slab thickness was $0.6\rm a_0$ and the air hole radius $0.29\rm a_0$, as before. The calculated $E_y$ field is shown in Fig. 6(a) and the profile along the centerline [parallel to $x$, the solid line in Fig. 6(a)] is shown in Fig. 6(b). The envelope of the mode field matches the Gaussian function very closely. The calculated $Q$-factor and the modal volume are $5 \times 10^8$ and $1.3(\lambda/n)^3$, respectively, which corresponds to a 25-fold increase of the theoretical $Q$-factor while maintaining the same modal volume. By comparing Fig. 6(a) with Fig. 3(c), it is apparent that the mode field of the new cavity extends further along the $x$-direction (parallel to the waveguide), which is expected to result in the suppression of losses from the cavity. Moreover, the mode field extension in the $y$-direction is smaller in the new cavity because the guiding mechanism is based on refractive index guiding, leading to the same modal volume as in the previous multiheterostructure nanocavity design, despite the extension of the mode field in the $x$-direction. Fig. 6(c) shows the calculated 2D FT of electric field of this cavity, which clearly shows that almost no components exist inside the leaky region. The small mode field extension in the $y$-direction leads to the extension of the FT components in the $k_y$ direction However, this does not cause

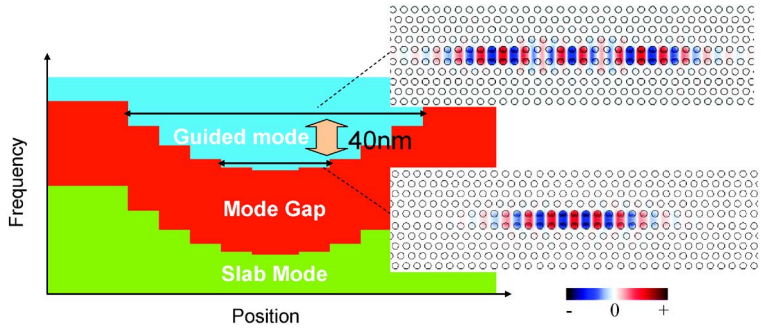


Fig. 7. Calculated $E_y$ distributions of the fundamental and second-order resonant modes with a schematic picture of the band diagram along the waveguide direction. The free spectrum range is calculated to be 40 nm when the resonant wavelength is about 1.5 $\mu$m.

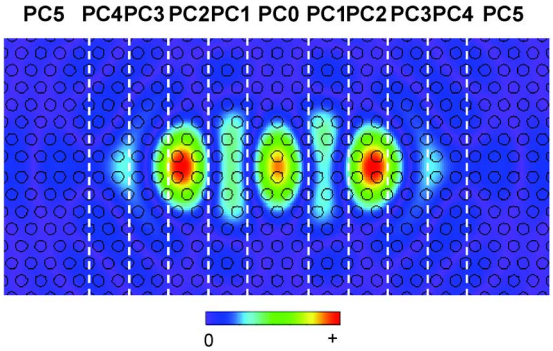


Fig. 8. Calculated distribution of the component responsible for leakage from the nanocavity.

the peaks to shift along $k_x$ and thus the shape of the mode along the $y$ axis is not a major influence on $Q$ factor. The higher-order mode of this cavity is shown in Fig. 7 beside the fundamental mode and band diagram. The free spectral range of this cavity is 40 nm when the resonant wavelength is $\sim 1.5\,\mu$m, which is 4 times larger than that of the previous multiheterostructure nanocavity. This result shows that single-mode operation is possible for a broad range of wavelengths.

To further increase the $Q$ factor, the positions from which the light leaks from the cavity are investigated. The leaky component of the nanocavity corresponds to the FT component inside the leaky region [see Fig. 6(c)]. Therefore, the leaky positions can be derived by the following method: The FT components inside the leaky region shown in Fig. 6(c) are isolated and only these components are inverse Fourier transformed. Fig. 8 shows the resulting distribution responsible for leakage, which is clearly largest in the PC2 region with an additional smaller component in the PC0 region. Therefore, we adjusted $a_2$ and repeated this process. By this optimization process, we have found that a $Q$-factor of $7 \times 10^8$, almost $10^9$, with modal volume of $1.3(\lambda/n)^3$ can be achieved by use of a 6-step multiheterostructure with lattice constants of $a_1 = 0.998a_0, a_2 = 0.993a_0, a_3 = 0.985a_0, a_4 = 0.975a_0, a_5 = 0.961a_0$, and $a_6 = 0.945a_0$.

## IV. Conclusion

In this paper, we have discussed approaches to designing 2 D PC nanocavities with high-$Q$. The most important consideration is to achieve strong photon confinement in the out-of-plane direction of the 2D PC, which can be realized using a Gaussian mode profile. We then discussed the analytical design of a nanocavity with an even Gaussian mode profile. We have designed successfully a nanocavity with a $Q$-factor of almost $10^9$ while maintaining the same modal volume of $1.3(\lambda/n)^3$, based on a waveguide with refractive index guiding. This cavity has a theoretical photon lifetime of $\sim 1\,\mu$s and can thus potentially be applied to a range of technologies, including an optical buffer memory for optical telecommunications.

## References

[1] Y. Akahane, T. Asano, B. S. Song, and S. Noda, "High-$Q$ photonic nanocavity in a two-dimensional photonic crystal," *Nature*, vol. 425, pp. 944–947, Oct. 2003.

[2] Y. Akahane, T. Asano, B. S. Song, and S. Noda, "Fine-tuned high-$Q$ photonic-crystal nanocavity," *Opt. Express*, vol. 13, pp. 1202–1214, Feb. 2005.

[3] B. S. Song, S. Noda, T. Asano, and Y. Akahane, "Ultra-high-$Q$ photonic double-heterostructure nanocavity," *Nature Mater.*, vol. 4, pp. 207–210, Mar. 2005.

[4] T. Asano, B. S. Song, Y. Akahane, and S. Noda, "Ultrahigh-$Q$ nanocavities in two-dimensional photonic crystal slabs," *IEEE J. Sel. Topics Quantum Electron.*, vol. 12, pp. 1123–1134, Dec. 2006.

[5] E. Kuramochi, M. Notomi, S. Mitsugi, A. Shinya, T. Tanabe, and T. Watanabe, "Ultrahigh-$Q$ photonic crystal nanocavities realized by the local width modulation of a line defect," *Appl. Phys. Lett.*, vol. 88, p. 041112, Jan. 2006.

[6] S. Noda, M. Fujita, and T. Asano, "Spontaneous-emission control by photonic crystals and nanocavities," *Nature Photon.*, vol. 1, pp. 449–458, Aug. 2007.

[7] Y. Takahashi, H. Hagino, Y. Tanaka, B. S. Song, T. Asano, and S. Noda, "High-$Q$ nanocavity with a 2-ns photon lifetime," *Opt. Express*, vol. 15, pp. 17206–17213, Dec. 2007.

[8] T. Yoshie, A. Scherer, J. Hendrickson, G. Khitrova, H. M. Gibbs, G. Rupper, C. Ell, O. B. Shchekin, and D. G. Deppe, "Vacuum Rabi splitting with a single quantum dot in a photonic crystal nanocavity," *Nature*, vol. 432, pp. 200–203, Nov. 2004.

[9] S. Noda, "Seeking the ultimate nanolaser," *Science*, vol. 314, pp. 260–261, Oct. 2006.

[10] Y. Tanaka, J. Upham, T. Nagashima, T. Sugiya, T. Asano, and S. Noda, "Dynamic control of the $Q$ factor in a photonic crystal nanocavity," *Nature Mater.*, vol. 6, pp. 862–865, Sep. 2007.

[11] M. F. Yanik and S. Fan, "Stopping light all optically," *Phys. Rev. Lett.*, vol. 92, p. 083901, Feb. 2004.

[12] S. Strauf, K. Hennessy, M. T. Rakher, Y.-S. Choi, A. Badolato, L. C. Andreani, E. L. Hu, P. M. Petroff, and D. Bouwmeester, "Self-tuned quantum dot gain in photonic crystal lasers," *Phys. Rev. Lett.*, vol. 96, p. 127404, Mar. 2006.

[13] M. Nomura, S. Iwamoto, K. Watanabe, N. Kumagai, Y. Nakata, S. Ishida, and Y. Arakawa, "Room temperature continuous-wave lasing in photonic crystal nanocavity," *Opt. Express*, vol. 14, pp. 6308–6315, Jun. 2006.

[14] S. Noda, A. Chutinan, and M. Imada, "Trapping and emission of photons by a single defect in a photonic bandgap structure," *Nature*, vol. 407, pp. 608–610, Oct. 2000.

[15] B. S. Song, S. Noda, and T. Asano, "Photonic devices based on in-plane hetero photonic crystals," *Science*, vol. 300, p. 1537, Jun. 2003.
[16] H. Takano, B. S. Song, T. Asano, and S. Noda, "Highly efficient multi-channel drop filter in a two-dimensional hetero photonic crystal," *Opt. Express*, vol. 14, pp. 3491–3496, Apr. 2006.
[17] M. J. Hartmann, F. G. S. L. Brandão, and M. B. Plenio, "Strongly interacting polaritons in coupled arrays of cavities," *Nature Phys.*, vol. 2, pp. 849–855, Dec. 2006.
[18] K. Hennessy, A. Badolato, M. Winger, D. Gerace, M. Atature, S. Gulde, S. Falt, E. L. Hu, and A. Imamoglu, "Quantum nature of a strongly coupled single quantum dot-cavity system," *Nature*, vol. 445, pp. 896–899, Feb. 2007.
[19] Y. Akahane, M. Mochizuki, T. Asano, Y. Tanaka, and S. Noda:, "Design of a channel drop filter by using a donor-type cavity with high-quality factor in a two-dimensional photonic crystal slab," *Appl. Phys. Lett.*, vol. 82, pp. 1341–1343, Mar. 2003.
[20] Y. Akahane, T. Asano, B. S. Song, and S. Noda:, "Investigation of high-$Q$ channel drop filters using donor-type defects in two-dimensional photonic crystal slabs," *Appl. Phys. Lett.*, vol. 83, pp. 1512–1514, Aug. 2003.
[21] K. Srinivasan, P. E. Barclay, O. Painter, J. Chen, A. Y. Cho, and C. Gmachl, "Experimental demonstration of a high quality factor photonic crystal microcavity," *Appl. Phys. Lett.*, vol. 83, pp. 1915–1917, Sep. 2003.
[22] W. Kohn, "Analytic properties of Bloch waves and Wannier functions," *Phys. Rev.*, vol. 115, pp. 809–821, Aug. 1959.
[23] B. S. Song, T. Asano, and S. Noda, "Physical origin of the small modal volume of ultra-high-$Q$ photonic double-heterostructure nanocavities," *New J. Phys.*, vol. 8, p. 209, Sep. 2006.
[24] M. Notomi, K. Yamada, A. Shinya, J. Takahashi, C. Takahashi, and I. Yokohama, "Extremely large group-velocity dispersion of line-defect waveguides in photonic crystal slabs," *Phys. Rev. Lett.*, vol. 87, p. 253902, Dec. 2001.

**Yoshinori Tanaka** received the B.S., M.S., and Ph.D. degrees from Kyoto University, Kyoto, Japan, in 2001, 2003, and 2006, respectively, all in electronics.

From 2003 to 2006, he was a Research Fellow with the Japan Society for the Promotion of Science, Kyoto University, where, from 2006 to 2007, he was a Postdoctoral Fellow, and, since 2007, is an Assistant Professor of the Global COE program in the Department of Electronic Science and Engineering. His current research interests include the 2-D photonic crystals.

Dr. Tanaka is a member of the Japan Society of Applied Physics.

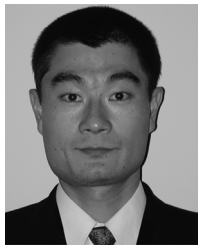

**Takashi Asano** received the B.S., M.S., and Ph.D. degrees from Kyoto University, Kyoto, Japan, in 1992, 1994, and 1997, respectively, all in electronics.

From 1996 to 1998, he was a Research Fellow with the Japan Society for the Promotion of Science at Kyoto University. From 1999 to 2000, he was a Postdoctoral Fellow at the Kyoto University Venture Business Laboratory, Kyoto. He joined Kyoto University, in 2000, and is currently an Associate Professor in the Department of Electronic Science and Engineering. His research has been concerned with intersubband transitions in quantum wells, ultrafast phenomena in semiconductors, and 2-D photonic crystals. His current research interests include defect engineering and light—matter interaction in semiconductor-based 2-D photonic crystals.

Dr. Asano is a member of the Japan Society of Applied Physics.

**Susumu Noda** (M'92–SM'06–F'08) received the B.S., M.S., and Ph.D. degrees from Kyoto University, Kyoto, Japan, in 1982, 1984, and 1991, respectively, all in electronics. He received an honorary degree from Gent University, Gent, Belgium, in 2006.

From 1984 to 1988, he was with the Mitsubishi Electric Corporation, where he was engaged in research on optoelectronic devices including AlGaAs/GaAs distributed-feedback (DFB) lasers and multiple-quantum-well DFB lasers. In 1988, he joined Kyoto University where he is currently a Professor in the Department of Electronic Science and Engineering and a Director of the Center of Excellence for Education and Research on Photonics and Electronics Science and Engineering. His research interest covers physics and applications of photonic and quantum nanostructures.

Prof. Noda is a Fellow of the Japan Society of Applied Physics (JSAP), and a member of the Institute of Electronics, Information, Communication Engineers (IEICE) and the Laser Society of Japan. He is the recipient of various awards, including the IBM Science Award (2000), the JSAP Achievement Award on Quantum Electronics (2005), and Optical Society of America Joseph Fraunhofer Award/Robert M. Burley Prize. From 2003 to 2005, he served as an IEEE Lasers and Electro-Optics Society (LEOS) Distinguished Lecturer. Since 2007, he has served as an IEEE/LEOS Kansai Chapter Chairman.